Frequency Control of Shipboard Microgrid Using a Novel Artificial Rabbits Optimization Tuned Cascaded PI-TID Controller

Smriti Jaiswal*‡, Manas Jyoti Mahanta*, Subash Chandra Sahoo*,
Kothalanka K Pavan Kumar*, Dulal Chandra Das *

* Department of Electrical Engineering, National Institute of Technology Silchar, Silchar, Assam, India-788010

(smriti_rs@ee.nits.ac.in, manasmahanta877@gmail.com, subash_rs@ee.nits.ac.in, kothalanka_rs@ee.nits.ac.in, dulal@ee.nits.ac.in)

‡ Corresponding Author: Smriti Jaiswal, Research scholar, Electrical Engineering Department, National Institute of Technology Silchar, Silchar, Assam, India-788010, smriti_rs@ee.nits.ac.in

Received: 17.01.2025 Accepted:18.03.2025

Abstract- This paper proposes a novel meta-heuristic technique to investigate frequency deviation control for the multi-energy model designed for a secluded shipboard microgrid system. This marine commercial vessel design is equipped with renewable energy resources like wind turbine generator, solar PV array, sea wave energy generator, biogas generator, biodiesel generator, aqua electrolyzer, proton exchange membrane fuel cell, and ultra-capacitor. This study aims to enhance the proposed system's performance and mitigate frequency variations using a novel Artificial Rabbits' Optimization method with a cascaded PI-TID controller. Further, for viability validation of the selected controller, a hardware-in-the-loop simulation based on OPAL-RT is executed to analyze real-time scenarios in several case studies. The results of this study provide a comparative assessment of novel technique proposed in contrast to the results of existing well-established techniques like Grasshopper Optimization Algorithm, Particle Swarm Optimization, Sine Cosine algorithm, and Salp Swarm Optimization Algorithm. The outcomes demonstrate the viability of the proposed SMG and the suitability of the selected controller over PID and TID controllers in preserving frequency stability in real-time.

Keywords Artificial rabbits optimization, biogas generator, load frequency control, proportional integral tilt integral-derivative controller, shipboard microgrid.

1. Introduction

Advanced technologies such as cleaner fuel sources and energy storage are of prime importance for achieving ships' cost and emissions reduction targets under international marine pollution regulations. In the wake of changing environmental rules, smart grids and AC/DC shipboard microgrid (SMG) technologies must drive efficiency and control. Over 80% of world trade depends on maritime shipping, which operates mainly on diesel engines. Consistent with IMO's Vision 2023, the aim is to reduce ship greenhouse gas emissions by 30% by 2030 and at least 70%-80% by 2040 [1]. Introducing significant indexes for short-term GHG reduction like technical Energy Efficiency Existing Ship Index (EEXI), operational Carbon Intensity Indicator (CII), and an enhanced Ship Energy Efficiency Management Plan are significantly revised strategies at its initial stage [2]. To restrain environmental pollution, the target range of possible technical & operational solutions estimated under IMO strategy for ships with, Greenhouse gases (GHGs) reduction potential is 10% for voltage optimization and another 10% for energy management [1]. For global warming mitigation of greenhouse gases, land and shipboard microgrids increasingly have renewable energy sources (RESs) integrated into them. In naval applications, shipboard microgrids—are AC/DC based on their topology—include power electronics, battery storage, energy management, load control, and communication systems [3,4]. Research is extensive for load frequency control (LFC) in RES-integrated energy storage-based shipboard microgrids [5]. A VOSviewer analysis (2015-2025) of 461 studies identifies some major trends, such as frequency control, energy storage, converters, renewable resources, marine vehicles, ship propulsion load, and DC microgrids (Fig. 1) [6].

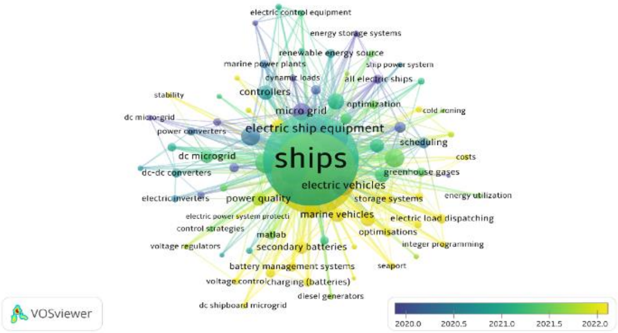

Fig. 1. Co-occurrence analysis for shipboard microgrid based articles reported within year 2015-2025.

Shipboard microgrids need to be protected from overloads, loads, and reconfiguration for safe operation. Voltage regulation and frequency regulation still pose challenges in dynamic-load hybrid microgrids with random RESs [7]. Frequency-division power sharing optimizes prime movers and energy storage, while fractional-order controllers and optimization support frequency regulation [8]. Hierarchical frequency regulation, such as droop regulation and frequency error integral control, is used in islanded SMGs [9]. Coordinated SPV-battery control uses methods such as Weibull M-transform least mean square (WMLMS) and frequency-fixed complex filter-based quasi-type-1 phase-locked loop (FFCF-QT1-PLL) to suppress harmonics [10]. Time-delayed secondary load frequency control overcomes communication delays and oscillations [11]. Improved black hole optimization improves fractional-order fuzzy PD+I controllers [12]. One of the challenging aspects of hybrid ship power systems is scheduling solar, wind, and sea wave energy using power management systems (PMS) [13,14]. Sea wave energy (2-3 kW/m²) is more potential than wind (0.5 kW/m²) and solar (0.1-0.3 kW/m²) [15]. Cruise ships produce food waste on a daily basis, an opportunity for biogas-based SMG integration [16-18]. Hybridization with biogas using SPV and wind energy enhances efficiency [19,20]. Stand-alone SMGs have more frequent regulation issues compared to grid-tied microgrids. The integration of energy storage improves power quality [21]. Proper management of power and energy storage reduces fuel consumption [22]. Ultracapacitors level off shipboard microgrid fluctuations [23]. Technological advancements in SMG technology and power quality control have been researched intensively [24]. Frequency stability in maintaining it using optimized load frequency control (LFC) reduces fuel consumption [25]. Traditional controllers such as PI [26] and PID [27] are challenged by sporadic RESs [28]. Fractional-order controllers enhance performance [29], though complexity in tuning remains. Options include sliding mode control (SMC) [30], model predictive control (MPC) [31], fractional-order MPC (FOMPC) [32], and robust control [33]. The tilt integral derivative (TID) controller, a sophisticated PID type, improves tuning and disturbance rejection [34]. TID-based controllers, such as fuzzy PD-TID, enhance stability [35-37]. The objective and contribution of study are:

1. Establish a transfer function model for an isolated SMG incorporating solar PV (SPV) array, sea wave energy (SWE) generator, biogas generator (BGG), biodiesel generator (BDG), aqua electrolyzer (AE), proton exchange membrane fuel cell (PEMFC), wind turbine generator (WTG), and ultracapacitor (UC).
2. Tune controller parameters by the ARO algorithm and compare its performance with PSO, SSA, GOA, and SCA.
3. Compare ARO-optimized cascaded PI-TID, TID, and PID controllers in the proposed SMG.
4. Evaluate SMG performance under actual conditions, such as changing weather, SWE non-availability, RES intermittence, and load fluctuations.
5. Verify the chosen controller in real-time via an OPAL-RT-based HIL simulation.

Section 2 addresses system modeling, Section 3 addresses methodology, Section 4 reports simulation results, and Section 5 experimental validation and then concludes.

2. Modelling of The Proposed SMG

In the stand-alone SMG system, SPV, WTG, and SWE act as uncontrolled renewable sources, and BDG, BGG, PEMFC, and AE facilitate power flow management. UC, with high power density, compensates for abrupt frequency oscillations. The system balances supply and demand through optimal control of the energy source. Fig. 2 shows the block diagram, and Table 1 provides system nomenclatures and values. The subsequent subsections present each component.

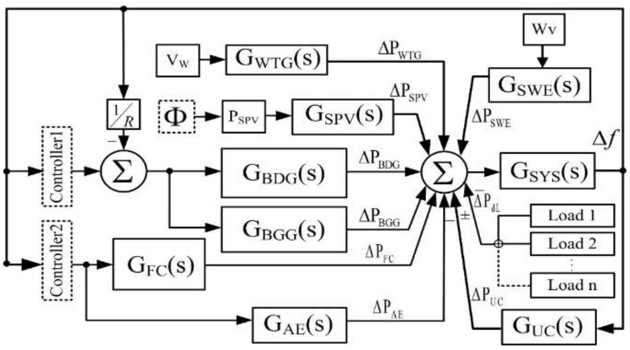

Fig. 2. Block diagram of the proposed SMG.

Table 1. System nomenclature and values

Symbol	Nomenclature	Values
T_{WTG}, K_{WTG}	WTG unit 's Time constant and gain	1.5s, 1
T_{SPV}, K_{SPV}	SPV unit 's Time constant and gain	1.8s, 1
T_{BE}, K_{BE}	BDG unit's Time constant and engine gain	0.5s, 1
T_{VA}, K_{VA}	Valve actuator delay and valve gain and of BDG unit	0.05s, 1
T_{WG}, K_{WG}	Wave the governor's time constant and gain	0.5s, 1
T_{WT}, K_{WT}	Wave turbine's time constant and gain of	4s, 1
X_C, Y_C, T_{CR}, b_B, T_{BT}, T_{BG}	lead time, lag time, combustion reaction delay, valve actuator delay, discharge time constant, and biogas delay of the BGG unit, respectively	0.6, 1s, 0.01s, 0.05, 0.2s, 0.23s
T_{FC}, K_{FC}	FC unit's Time constant and gain of	0.26s, 1
T_{filt}, K_{filt}	FC's interconnection device Time constant and gain	0.004s, 1
T_{inv}, K_{inv}	FC's inverter Time constant and gain	0.04s, 1
T_{UC}, K_{UC}	UC unit's Time constant and gain	0.9s, .7
T_{AE}, K_{AE}	AE unit's Time constant and gain	0.2s, 1
R	Droop constant in Hz/p.u.	2
M	Inertia constant for the system	0.2s
D	The damping factor in p.u. MW/Hz	0.012
ΔP_{dL}	The net change in load power in p.u.	-
Δf	Frequency deviation of the system in Hz	-

2.1. Solar PV

SPV arrays produce electricity directly from sunlight through the photovoltaic effect. Solar irradiance (Φ in kW/m²) and cell surface temperature (Ta in °C) are the most significant factors affecting output power (eq. A1) [44]. With a surface area of 4084 m² and a conversion efficiency of 0.09–0.12 [45], the SPV's linearized response in the low-frequency range is expressed as a first-order transfer function Eq. (1,2) [46].

$$P_{PV} = \eta S\left\{1-.005\left(25+T_a\right)\right\}\Delta\Phi \tag{1}$$

$$G_{SPV}(s) = \frac{K_{SPV}}{1+sT_{SPV}} \tag{2}$$

2.2. Wind Turbine Generator

Wind turbine power varies with wind velocity in the cut-in and cut-out range, and a pitch mechanism aligns blade angles to avoid excess generation [18,40]. Its power output by air density, power coefficient, wind speed, and blade area is mathematically formulated as in Eq. (3), and its transfer function response is expressed in Eq. (4) [20,40].

$$P = \frac{1}{2}\rho C_P A V_W^3 \tag{3}$$

$$G_{WTG}(s) = \frac{K_{WTG}}{1+sT_{WTG}} \tag{4}$$

2.3. Aqua Electrolyzer

Surplus energy from RESs is stored in the form of hydrogen by AE, which is subsequently used by the fuel cell to produce power in periods of low production. An AE-fitted fuel cell incorporated in the MG serves to decrease power fluctuations, whose transfer function is provided as Eq. (5) [47].

$$G_{AE}(s) = \frac{K_{AE}}{1+sT_{AE}} \tag{5}$$

2.4. Proton Exchange Membrane Fuel Cell

Fuel cells are utilized owing to their large energy density and low emissions [46-49], and PEMFC is utilized here because it has a rapid startup, low operating temperature, and is eco-friendly. DC is converted into AC through an inverter and the PEMFC transfer function is expressed in Eq. (6) [50,51].

$$G_{PEMFC}(s) = \left(\frac{K_{FC}}{1+sT_{FC}}\right)\left(\frac{K_{inv}}{1+sT_{inv}}\right)\left(\frac{K_{filt}}{1+sT_{filt}}\right) \tag{6}$$

2.5. Biogas Generator

The growing cruise industry has led to increased solid waste discharge, posing environmental concerns [49]. Utilizing onboard organic waste for biogas generation via anaerobic digestion can enhance the ship's energy system, with the BGG transfer function given in Eq. (7) [6,52,53].

$$G_{BGG}(s) = \left(\frac{1+sX_C}{(1+sY_C)(1+sb_B)}\right)\left(\frac{1+sT_{CR}}{1+sT_{BG}}\right)\left(\frac{1}{1+sT_{BT}}\right) \tag{7}$$

2.6. Sea Wave Energy Generator

Sea wave energy, harnessed by wave energy converters for shipboard microgrids, offers high potential but poses frequency instability due to its fluctuating nature, with the transfer function given in Eq. (8) [3,17].

$$G_{SWE}(s)=\left(\frac{K_{WG}}{1+sT_{WG}}\right)\left(\frac{K_{WT}}{1+sT_{WT}}\right) \tag{8}$$

2.7. Biodiesel Generator

Biodiesel, which is made through trans-esterification of vegetable oils and crops, is a green diesel substitute with great air quality, biodegradability, and non-toxicity, thus making BDG an appropriate option in this work, whose transfer function is provided in Eq. (9) [38].

$$G_{BDG}(s)=\left(\frac{K_{VA}}{1+sT_{VA}}\right)\left(\frac{K_{BE}}{1+sT_{BE}}\right) \tag{9}$$

2.8. Ultracapacitor

High-power-density ultracapacitors and rapid response ultracapacitors level power during switching loads and provide excess energy buffering in islanded microgrids [54–56]. They have a transfer function represented as Eq. (10) [37].

$$G_{UC}(s)=\left(\frac{K_{UC}}{1+sT_{UC}}\right) \tag{10}$$

2.9. Dynamic Modeling of SMG

The microgrid power variation is the generation demand difference [28], expressed by Eq. (11), whose transfer function is in Eq. (12).

$$\Delta P_{SMG}=\Delta P_{SPV}+\Delta P_{WTG}+\Delta P_{SWE}+\Delta P_{BGG}+\Delta P_{BDG}+\Delta P_{PEMFC}-\Delta P_{AE}\pm\Delta P_{UC}-\Delta P_{dL} \tag{11}$$

$$G_{SYS}(s)=\frac{\Delta f}{\Delta P_{SMG}}=\left(\frac{1}{D+sM}\right) \tag{12}$$

3. Methodology Assortment

3.1. Objective Function Formulation

While minimizing the system frequency variations by acquiring the optimum controller gains, the objective function has a crucial role. This LFC approach implements Integral square error (ISE) [29]. The objective function considering ISE is expressed as Eq. (13).

$$Minimize, J_{ISE}=\int_{0}^{t_{sim}}(\Delta f)^2.dt \tag{13}$$

$$Subject\ to,\begin{cases} K_{P\min}\le K_P\le K_{P\max}\\ K_{I\min}\le K_I\le K_{I\max}\\ K_{T\min}\le K_T\le K_{T\max}\\ K_{I\min}\le K_I\le K_{I\max}\\ K_{D\min}\le K_D\le K_{D\max}\\ n_{\min}\le n\le n_{\max}\end{cases} \tag{14}$$

Here, K_P, K_I, K_T, K_I, *and* K_D are the gain constants, and n is the tuning parameter of the cascaded PI-TID controller in Eq. (14).

3.2. Optimization Algorithm Selection

Optimization efficiently supports rapid controller parameter tuning, with the need for comparing the devised ARO algorithm [42] with available schemes. ARO is compared against PSO [29], GOA [27], SSA [32], and SCA [30] on LFC for the SMG employing a PID controller. Simulations consider simulation time, tsim=120 sec, maximum iteration, maxitr=100, and the total number of searching individuals, n=50, boundary limits [0,50]. ARO achieves the lowest objective function, Jmin= 0103128.0, faster with the smallest values of undershoot (-USH) and overshoot (+OSH). Table 2 reports comparative parameters, and Fig. 3 plots frequency deviation curves, which justify ARO's best performance. Metaheuristic algorithms efficiently handle optimization problems to obtain near-optimal solutions within complicated search spaces. Artificial Rabbit Optimization (ARO), taking cues from the foraging mechanism of rabbits, surpasses PSO and GOA in terms of convergence as well as resistance to local optima, but its adaptive search strategy renders it better than SSA and SCA for multimodal problems. Exploration and exploitation of ARO are balanced through adaptive control parameters (C1, C2, α, β) to avoid inefficiency at high dimensions in optimization. Its quick convergence and lower probability of local optima trapping make it very efficient in solving complex problems.

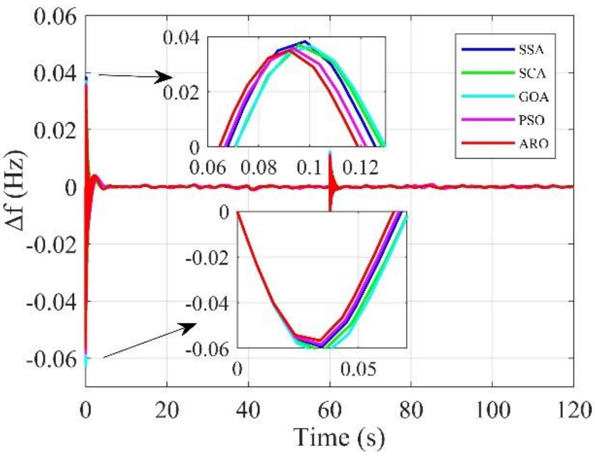

Fig. 3. Frequency response of competitive algorithms.

Table 2. Comparison of SCA, GOA, SSA, PSO, and ARO with parameter values

Algorithm's Parameter			Value
SCA	Exploration-Exploitation Control Parameter	a	[2-0]
	Position Update Factor	r	[0,1]
GOA	Convergence Factor	c	[1-0]
	Attraction Force	f	[0,1]
	Repulsion Distance	d	0.15
SSA	Exploration Control Factor	ec	[2-0]
	Leader-Follower Role Division	l	0.5
PSO	Inertia Weight	w	[0.95-1]
	Cognitive Coefficient	c1	[1.5–2.5]
	Social Coefficient	c2	[1.5–2.5]
	Velocity Update Factor	v	[0.1-0.2]
ARO	Exploration Parameter	C1	[0.1, 1.5]
	Exploitation Parameter	C2	[0.1, 1.5]
	Adaptive Movement Factor	α	[0.1, 2.0]
	Learning Factor	β	[0.1, 2.0]

3.3. Overview of the ARO Algorithm

ARO is a new metaheuristic based on rabbits' survival tactics, mainly detour searching and random hiding [54]. In order to defend their burrows, rabbits search remotely from them and choose burrows at random in order to avoid predators. The switching among the strategies relies on their energy levels [42]. Using these tendencies, ARO enhances problem-solving effectiveness. Fig. 4 presents the flowchart of ARO, and the following subsections elaborate each step.

3.3.1. Detour Foraging

The detour foraging strategy is an exploration, where rabbits forage for food around other rabbits' nests and move towards randomly selected individuals in the swarm and update their positions relative to them. This is mathematically described by the following equations.

$$X_i(t+1) = Y_j(t) + R \cdot (Y_i(t) - Y_j(t)) + round(0.5 \cdot (0.05 + a_1)) \cdot n_1$$

Where, i,j = 1,2,…..n and i ≠ j (15)

Here t is the present iteration. Positions of i^{th} rabbit at (t+1) and t time are represented by $X_i(t+1)$ and Y_i, respectively. In Eq. (15), rabbit population n, d defines the problem's dimensions with T_{max}, highest iteration.

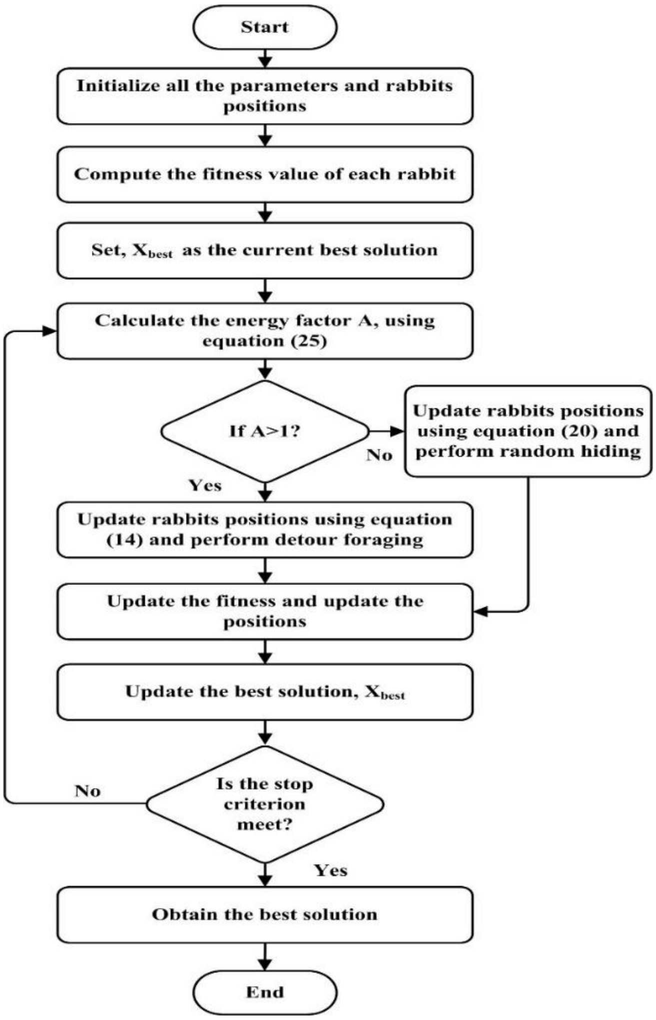

Fig. 4. Flowchart of ARO.

3.3.2. Random Hiding

Rabbits create multiple burrows near their nests and randomly select one to escape predators, making this hiding tactic a form of exploitation. The *j*th burrow of the *i*th rabbit is represented as bi,j(t), with a randomized perturbation while hiding factor P is linearly reduced from 1 to 1/T, and a4, and a5 are random nos. between [0,1] in Eq. (16,17).

$$b_{i,j}(t) = Y_i(t) + P \cdot g \cdot Y_i(t); \quad (16)$$

Where i=1, 2,…n and j=1,2,…d

$$P = \frac{T_{\max} - t + 1}{T_{\max}} \cdot a_5 \tag{17}$$

3.3.3. Energy Shrink

The energy factor determines whether a rabbit continues detour foraging or switches to random hiding, with higher values indicating endurance and lower values triggering hiding, as modeled in Eq. (18).

$$A(t) = 4\left(1 - \frac{t}{T_{\max}}\right)\ln\frac{1}{a} \tag{18}$$

3.4. Controllers Selection

Optimization of the controller is needed to ensure system performance. The work in this paper compares PID, TID, and PI-TID controllers using parameters optimized with ARO, an algorithm superior to other algorithms as in Eq. (19-20) [57-59]. Convergence plots validate that PI-TID tuned with ARO converges more quickly than PID and TID. It can be observed from Fig. 5 and Table 3 that PI-TID has the minimum overshoot of 0.02348, establishing its superiority. As compared to PID, TID substitutes a tilted proportional gain ($1/S^{1/n}$) in place of proportional gain with improved tuning and disturbance rejection. As a remedy for overcoming PID's oscillations and stability problems during transient, a cascaded PI-TID controller is proposed whose frequency response is in Fig. 6(a) and structure is in Fig. 6(b).

$$G_{PI} = K_P + \frac{K_I}{s} \tag{19}$$

$$G_{TID} = \frac{K_T}{s^{\frac{1}{n}}} + \frac{K_I}{s} + sK_D \tag{20}$$

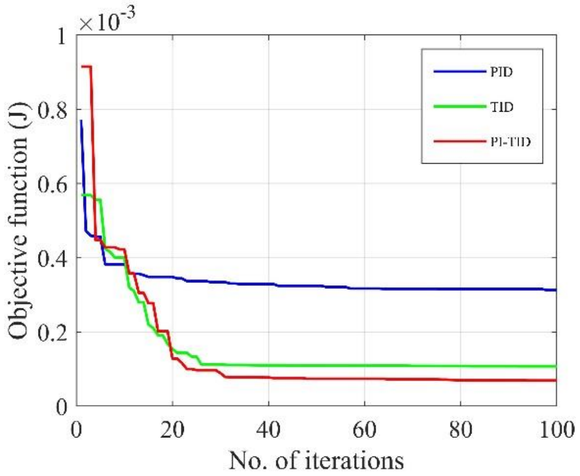

Fig.5. Convergence plots of traditional and hybrid controllers.

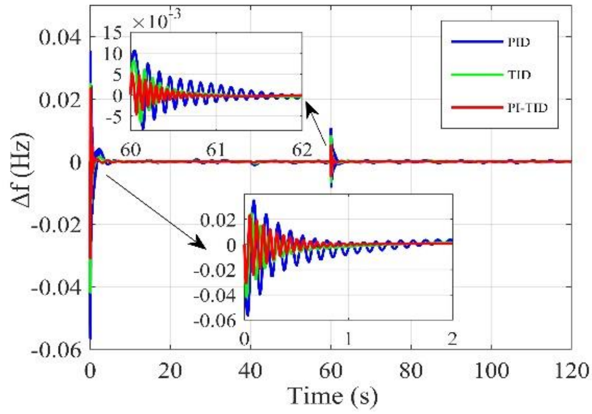

(a)

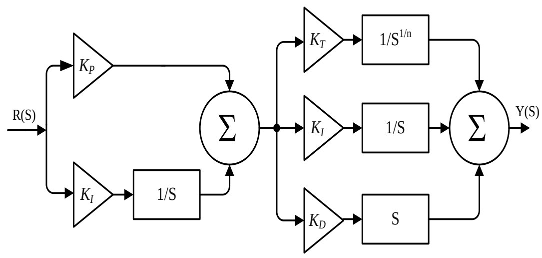

(b)

Fig. 6. (a) Frequency response of controllers **(b)** Cascaded PI-TID controller structure.

Table 3: Decision parameters for algorithms and controllers

	Algorithms/Controller	**$+O_{SH}$ (Hz)**	**$-U_{SH}$ (Hz)**	**J_{min}**
Algorithms	SCA	0.0370	0.0611	0.000411
	GOA	0.0366	0.0627	0.000361
	SSA	0.0382	0.0592	0.000354
	PSO	0.0357	0.0582	0.000332
	ARO	0.0350	0.0565	0.000312
Cont.	PID	0.0350	0.0565	0.000312
	TID	0.0248	0.0418	0.000107
	PI-TID	0.0234	0.0308	0.000069

4. Simulation Results and Discussions

MATLAB/Simulink (2023b) simulates the marine microgrid system to compare ARO-optimized PI-TID controller with controllers TID and PID. As the PI-TID controller is superior, it is employed in additional case studies with uncontrollable RESs such as SPV, WTG, and SWE, which are subject to climatic variations. The following subsections discuss the frequency responses of the proposed SMG model under various climatic conditions.

4.1. Case 1: Normal Day Conditions

In this scenario, all sources are in hand to serve load demand, with good weather guaranteeing 85.6% contribution from RESs. BDG, BGG, and PEMFC provide the balance energy, and UC regulates frequency spikes, absorbing 25.7–41.6% of demand fluctuations. Fig. 7(a) illustrates frequency oscillation within ±0.01 Hz as a result of a step load change from 0.2 to 0.25 p.u. at 60 sec.

4.2. Case 2: Cloudy/Nighttime Conditions

At night or during cloudy weather, the SPV unit is inactive, but all other generators remain operational. BDG and BGG handle 50.5–62.7% of demand, increasing their output by 80.1–90.3% to compensate for the SPV shortfall. UC stabilizes frequency deviations, which remain within ±0.00072 Hz at spikes and ±0.01 Hz overall, as shown in Fig. 7(b).

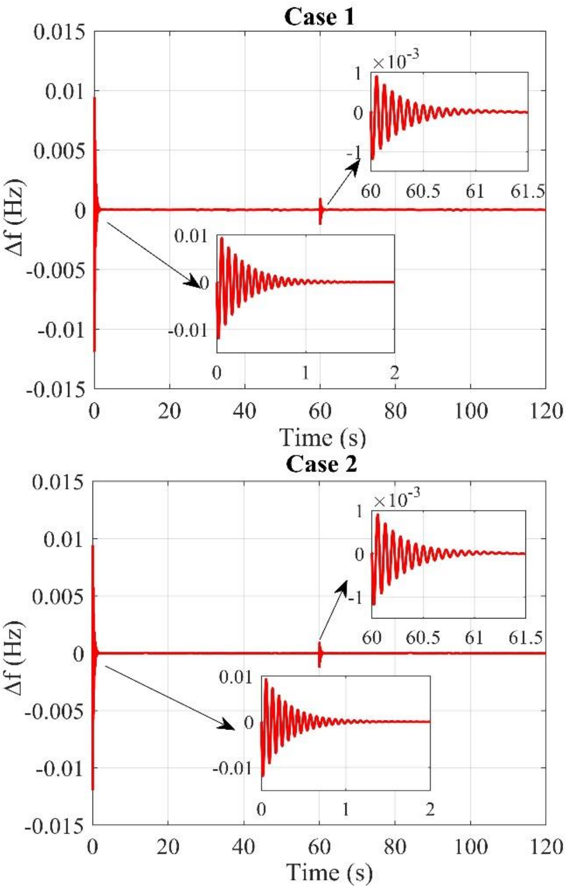

Fig. 7. (a). Frequency response under normal day conditions. **(b)**. Frequency response plot under cloudy/nighttime conditions.

4.3. Case 3: Windy/Gusty Conditions

With the WTG unit under shut-down under gusty weather, other RESs provide energy, with BDG and BGG getting ample fuel. BDG, BGG, and PEMFC units take the place of WTG by meeting 85.7–92.5% demand, while UC takes care of 7.1–14.3% to balance frequency. Fig. 8(a) indicates frequency response, sustaining deviations within ±0.0015 Hz in step load variation and ±0.0065 Hz in sharp spikes.

4.4. Case 4: SWE is Not Available

With the WTG unit not operating due to severe weather, SPV and WTG provide 45.6% and 32.4% of total generation, respectively, under case 1-like conditions. BDG, BGG, and PEMFC make up for the lack of the SWE unit by providing up to 10.08%, 7.05%, and 5.04% extra power. The UC unit regulates frequency oscillations, keeping them in ±0.00081 Hz during abrupt peaks, as illustrated in Fig. 8(b).

4.5. Case 5: Unavailability of Uncontrolled RESs

Under poor climatic or maintenance conditions, SPV, WTG, and SWE units are idle, with BDG, BGG, and PEMFC providing 31.20%, 23.40%, and 15.60% of the total power, respectively. The UC unit offers 7.80% to support rapid change in load, reducing frequency deviations and maintaining system stability. The frequency response is demonstrated in Fig. 9(a), keeping the variation between ±0.00093 Hz during sudden spikes.

4.6. Case 6: Random Load Variations

The model uses variable loading every 20 seconds to mimic real-time conditions, with all available sources. The excess energy from uncontrolled RESs is stored by the AE unit. Fig. 9(b) verifies system robustness since frequency fluctuations are within ±0.005 Hz despite ongoing random loading changes at 20-second intervals.

4.7. Real-time Analysis

A real-time OPAL-RT (OP4510) simulation of the proposed controller proves its feasibility. The OPAL-RT setup in Fig. 10 consists of a simulator OP4510, control station PC, and DSO for real-time display [45,60]. The frequency response in Fig. 11(a) coincides with the MATLAB result at 0.005 p.u./div. Fig. 11(b, c) validates system stability for a step load variation (0.36-0.365 p.u.) at 60 sec with energy contributions: BDG/BBG (0.1 p.u./div), SPV/SWE/WTG (0.05 p.u./div), and UC/AE (0.00015 p.u./div).

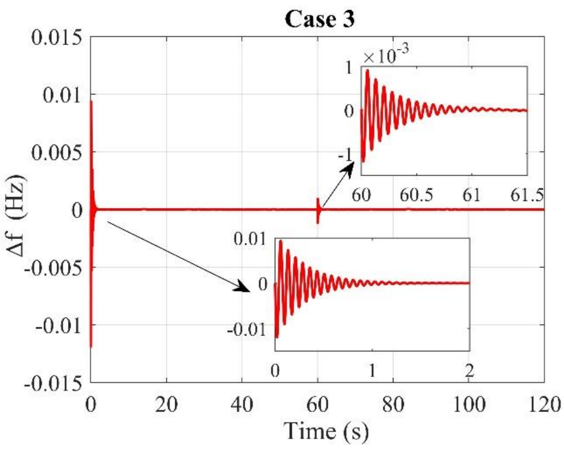

(a)

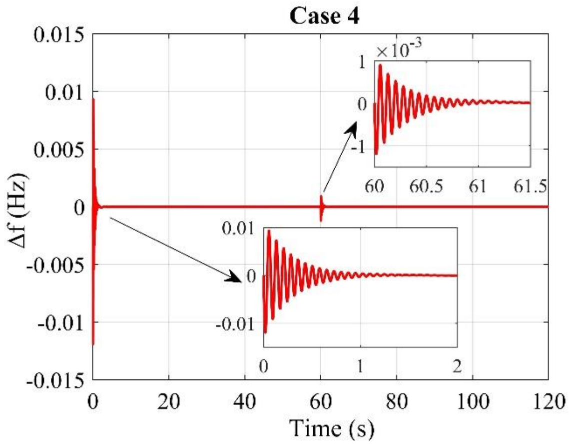

(b)

Fig. 8. (a) Frequency response under windy/gusty conditions. (b) Frequency response with SWE out of operation.

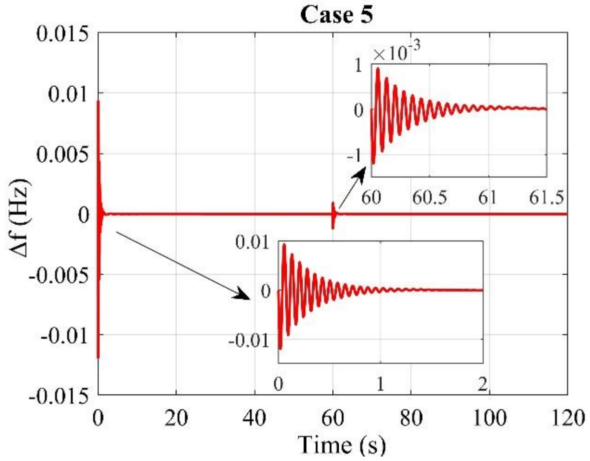

(a)

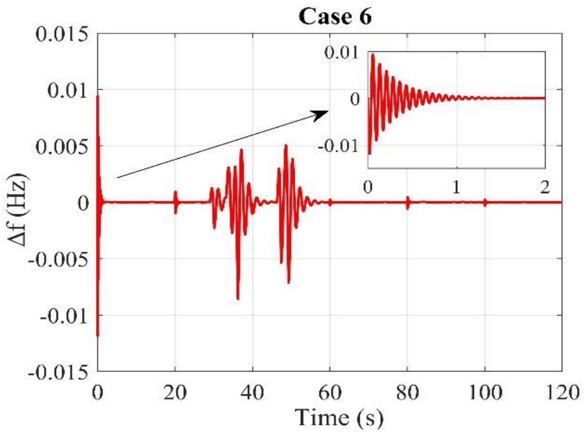

(b)

Fig. 9. (a) Frequency response when uncontrolled RESs are unavailable **(b)** Frequency response under random load variations.

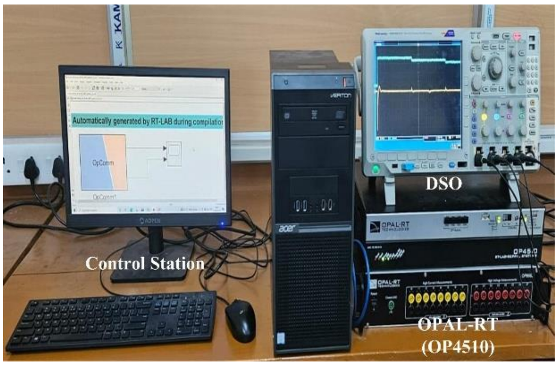

Fig. 10. OPAL-RT experimental setup, including real-time simulator and control station.

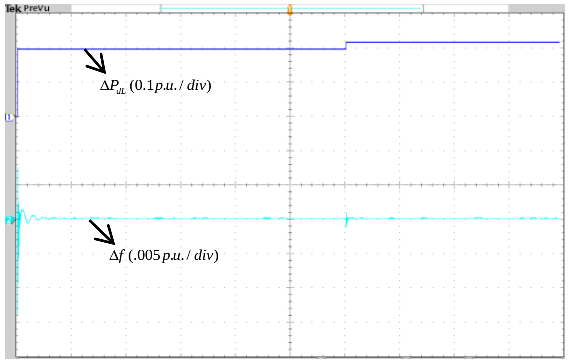

(a)

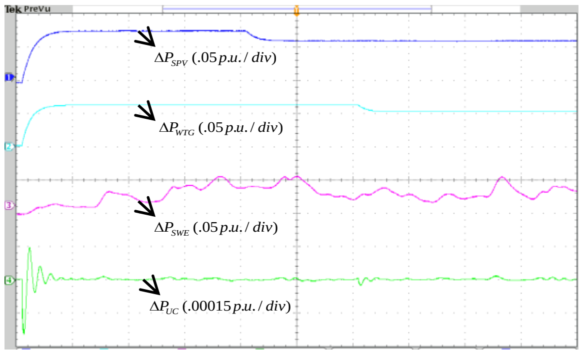

(b)

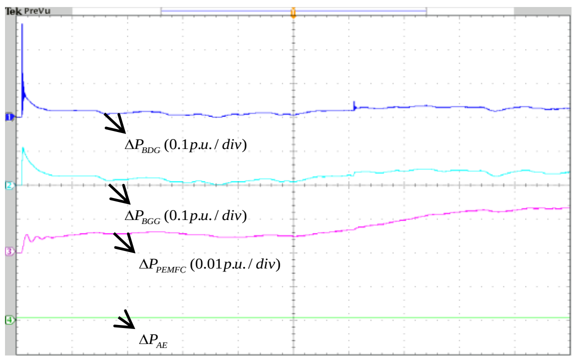

(c)

Fig. 11. (a) Load variations and corresponding frequency response, validating real-time controller performance. **(b)** Power distribution from SPV, WTG, SWE, and UC, showing variations in renewable generation. **(c)** Power contributions from controlled energy sources i.e., BDG, BGG, PEMFC, and AE.

5. Experimental Validation and Limitation

HIL simulation with OPAL-RT verifies the ARO-based PI-TID controller, allowing hardware-level testing prior to full-scale deployment and minimizing shipboard risks. The controller successfully stabilizes power by combining wind, solar, SWE, and biogas sources while performing better than conventional methods in frequency deviation. Real-world implementation is challenged by high computational complexity, necessitating optimization for real-time embedded execution. Communication delays, EMS nonlinearities, and industrial protocol latencies could also influence system response, requiring resilient implementation procedures. Marine environmental conditions such as vibration, temperature fluctuation, humidity, and corrosion can also affect sensor and controller stability.

6. Conclusion

This research presented an ARO-optimized cascaded PI-TID controller for LFC in a SPV, WTG, SWE, BGG, BDG, AE, PEMFC, and UC-powered SMG system. Comparative analysis with existing optimization methods (PSO, GOA, SSA, and SCA) validated its better performance, with the undershoot and overshoot being -0.03085 and 0.02348, respectively. The controller successfully kept the frequency deviations in acceptable ranges under different weather conditions, ensuring stability to the system. Real-time OPAL-RT HIL simulations also confirmed its viability, although real shipboard testing is still required. Nonetheless, the ARO method is computationally intensive, and real-time implementation on embedded systems without optimization is challenging. HIL simulation with OPAL-RT verifies the ARO-based PI-TID controller, allowing hardware-level testing prior to full-scale deployment and minimizing shipboard risks. The controller successfully stabilizes power by combining wind, solar, SWE, and biogas sources while performing better than conventional methods in frequency deviation. Real-world implementation is challenged by high computational complexity, necessitating optimization for real-time embedded execution. Communication delays, EMS nonlinearities, and industrial protocol latencies could also influence system response, requiring resilient implementation procedures. Marine environmental conditions such as vibration, temperature fluctuation, humidity, and corrosion can also affect sensor and controller stability. The PI-TID controller needs more flexibility for abrupt load changes, and hybrid optimization techniques may further improve its response. Future work should investigate AI-based adaptive tuning, shipboard microgrid security, and decentralized multi-agent control for enhanced system resilience and efficiency.

Acknowledgements

The authors acknowledge the support provided by National Institute of Technology Silchar for carrying out this work.

Appendix

Control parameter’s range of algorithms :

- PSO: W_{max}=1, W_{min}=0.99, C_1=1.5, C_2=2
- SCA: r_1=2-t(2/Maxitr), r_2=2π*rand (),
- r_3=2π*rand (), r_4=rand (),
- GOA: C_{max}=1, C_{min}=0.00004, L=1.5, f=0.5
- SSA: $C_1=2e^{(-4/Maxitr)2}$, C_2, C_3=rand [0,1]
- ARO: n, no,of candidates=50;

  Max_{itr}=, maximum no.of iterations=100

In the proposed SMG, the ratings of the selected components are SPV=250 kW, WTG=250 kW, SWE=100 kW, BGG=500 kW, BDG=500 kW, AE=100kW, PEMFC=100 kW, UC=50kW, with overall loading demand of 1000 kW.

References

[1] P. Xie, S. Tan, N. Bazmohammadi, J. M. Guerrero, and J. C. Vasquez, “A Real-Time Power Management Strategy for Hybrid Electrical Ships Under Highly Fluctuated Propulsion Loads,” IEEE Systems Journal, vol. 17, no. 1. Institute of Electrical and Electronics Engineers (IEEE), pp. 395–406, March, 2023.

[2] P. Pan, Y. Sun, C. Yuan, X. Yan, and X. Tang, “Research progress on ship power systems integrated with new energy sources: A review,” Renewable and Sustainable Energy Reviews, vol. 144. Elsevier BV, p. 111048, July, 2021.

[3] A. M. Aboelezz, B. E. Sedhom, M. M. El-Saadawi, A. A. Eladl, and P. Siano, “State-of-the-Art Review on Shipboard Microgrids: Architecture, Control, Management, Protection, and Future Perspectives,” Smart Cities, vol. 6, no. 3. MDPI AG, pp. 1435–1484, May ,2023.

[4] B. Babes, N. Hamouda, F. Albalawi, O. Aissa, S. S. M. Ghoneim, and S. A. M. Abdelwahab, “Experimental Investigation of an Adaptive Fuzzy-Neural Fast Terminal Synergetic Controller for Buck DC/DC Converters,” Sustainability, vol. 14, no. 13. MDPI AG, p. 7967, Jun. 29, 2022. doi: 10.3390/su14137967.

[5] Z. Jin, L. Meng, J. C. Vasquez, and J. M. Guerrero, “Frequency-division power sharing and hierarchical control design for DC shipboard microgrids with hybrid energy storage systems,” 2017 IEEE Applied Power Electronics Conference and Exposition (APEC). IEEE, pp. 3661–3668, March 2017.

[6] N. J. van Eck and L. Waltman, “Software survey: VOSviewer, a computer program for bibliometric mapping,” Scientometrics, vol. 84, no. 2. Springer Science and Business Media LLC, pp. 523–538, December, 2009.

[7] Microgrids: Control M. D. A. Al-Falahi, T. Tarasiuk, S. G. Jayasinghe, Z. Jin, H. Enshaei, and J. M. Guerrero, “AC Ship and Power Management Optimization,” Energies, vol. 11, no. 6. MDPI AG, p. 1458, June, 2018.

[8] W. F. Mbasso, S. R. D. Naoussi, R. J. J. Molu, S. K. Tsobze “Contribution into Robust Optimization of

Renewable Energy Sources: Case Study of a Standalone Hybrid Renewable System in Cameroon", International Journal of Renewable Energy Research, Vol.13, No.3, pp-1093-1118, September, 2023.

[9] A. Mondal, A. Latif, D. C. Das, S. M. S. Hussain, and A. Al-Durra, "Frequency regulation of hybrid shipboard microgrid system using butterfly optimization algorithm synthesis fractional-order controller," International Journal of Numerical Modelling: Electronic Networks, Devices and Fields, vol. 36, no. 5. Wiley, August, 2022.

[10] P. Semwal, V. Narayanan, B. Singh, and B. K. Panigrahi, "Control of Parallel Inverters for Electric Powered Shipboard Microgrid," 2022 IEEE 2nd International Conference on Sustainable Energy and Future Electric Transportation (SeFeT). IEEE, pp. 1–6, August, 2022.

[11] N. Vafamand, M. H. Khooban, T. Dragicevic, J. Boudjadar, and M. H. Asemani, "Time-Delayed Stabilizing Secondary Load Frequency Control of Shipboard Microgrids," IEEE Systems Journal, vol. 13, no. 3. Institute of Electrical and Electronics Engineers (IEEE), pp. 3233–3241, September, 2019.

[12] M.-H. Khooban, T. Dragicevic, F. Blaabjerg, and M. Delimar, "Shipboard Microgrids: A Novel Approach to Load Frequency Control," IEEE Transactions on Sustainable Energy, vol. 9, no. 2. Institute of Electrical and Electronics Engineers (IEEE), pp. 843–852, April, 2018.

[13] Shubham, S. P. Roy, R. K. Mehta, A. K. Singh, and O. P. Roy, "A novel application of jellyfish search optimisation tuned dual-stage (1 + PI)TID controller for microgrid employing electric vehicle," International Journal of Ambient Energy, vol. 43, no. 1. Informa UK Limited, pp. 8408–8427, July, 2022.

[14] P. Xie et al., "Optimization-Based Power and Energy Management System in Shipboard Microgrid: A Review," IEEE Systems Journal, vol. 16, no. 1. Institute of Electrical and Electronics Engineers (IEEE), pp. 578–590, March, 2022.

[15] B. Yildirim, "Gain and phase margins based stability region analysis of time-delayed shipboard microgrid with sea wave energy," IET Electric Power Applications, vol. 14, no. 8. Institution of Engineering and Technology (IET), pp. 1347–1359, June 2020.

[16] K. Schumüller, D. Weichgrebe, and S. Köster, "Biogas potential of organic waste onboard cruise ships — a yet untapped energy source," Biomass Conversion and Biorefinery, vol. 12, no. 12. Springer Science and Business Media LLC, pp. 5647–5662, January, 2021.

[17] R. B. Roy, S. Alahakoon, and S. G. Jayasinghe, "Microgrid and Fleet to Grid Operation of a Hybrid Electric Ferry," 2021 31st Australasian Universities Power Engineering Conference (AUPEC), vol. L 191. IEEE, pp. 1–6, September, 2021.

[18] M. Kotrikla, A. Zavantias, and M. Kaloupi, "Waste generation and management onboard a cruise ship: A case study," Ocean & Coastal Management, vol. 212. Elsevier BV, p. 105850, October. 2021.

[19] P. Sahoo and S. Panda, "Load Frequency Control of Solar Photovoltaic/Wind/Biogas/Biodiesel Generator Based Isolated Microgrid Using Harris Hawks Optimization," 2020 First International Conference on Power, Control and Computing Technologies (ICPC2T). IEEE, January. 2020.

[20] M. A. E. Eid, S. A. M. Abdelwahab, H. A. Ibrahim, and A. H. K. Alaboudy, "Improving the Resiliency of a PV Standalone System Under Variable Solar Radiation and Load Profile," in *2018 Twentieth International Middle East Power Systems Conference (MEPCON)*, IEEE, Dec. 2018, pp. 570–576, doi: 10.1109/mepcon.2018.8635160.

[21] U. N. Patel, H. H. Patel, "Dynamic Droop Control Method for Islanded Photovoltaic Based Microgrid for Active and Reactive Power Control with Effective Utilization of Distributed Generators," International Journal of Renewable Energy Research, no. v9i2. International Journal of Renewable Energy Research, Vol.9, No.2, pp. 1077-1088, 2019.

[22] E. Nivolianiti, Y. L. Karnavas, and J.-F. Charpentier, "Energy management of shipboard microgrids integrating energy storage systems: A review," Renewable and Sustainable Energy Reviews, vol. 189. Elsevier BV, p. 114012, January. 2024

[23] G. J. Tsekouras, F. D. Kanellos, and J. Prousalidis, "Simplified method for the assessment of ship electric power systems operation cost reduction from energy storage and renewable energy sources integration," IET Electrical Systems in Transportation, vol. 5, no. 2. Institution of Engineering and Technology (IET), pp. 61–69, June, 2015.

[24] M. U. Mutarraf, Y. Terriche, K. A. K. Niazi, F. Khan, J. C. Vasquez, and J. M. Guerrero, "Control of Hybrid Diesel/PV/Battery/Ultra-Capacitor Systems for Future Shipboard Microgrids," Energies, vol. 12, no. 18. MDPI AG, p. 3460, Sep. 07, 2019.

[25] S. Jayasinghe, L. Meegahapola, N. Fernando, Z. Jin, and J. Guerrero, "Review of Ship Microgrids: System Architectures, Storage Technologies and Power Quality Aspects," Inventions, vol. 2, no. 1. MDPI AG, p. 4, February. 15, 2017.

[26] A.Dkhil, J. Hmad, M. Amairi, M. Chetoui, and H. Trabelsi "Robust Fractional PI Controller Design for Stand-Alone Microgrid under Load Variation: An Optimization-Based Approach," International Journal of Renewable Energy Research, Vol.13, No.4, pp. 1526-1537, December, 2023.

[27] D. Ch. Das, A. K. Roy, and N. Sinha, "GA based frequency controller for solar thermal–diesel–wind hybrid energy generation/energy storage system," International Journal of Electrical Power & Energy Systems, vol. 43, no. 1. Elsevier BV, pp. 262–279, Dec. 2012.

[28] M. Bhuyan, A. K. Barik, and D. C. Das, “GOA optimised frequency control of solar-thermal/sea-wave/biodiesel generator based interconnected hybrid microgrids with DC link,” International Journal of Sustainable Energy, vol. 39, no. 7. Informa UK Limited, pp. 615–633, Mar. 16, 2020.

[29] P. Li, W. Hu, X. Xu, Q. Huang, Z. Liu, and Z. Chen, “A frequency control strategy of electric vehicles in microgrid using virtual synchronous generator control,” Energy, vol. 189. Elsevier BV, p. 116389, Dec. 2019

[30] Mondal, A. Latif, D. C. Das, S. M. S. Hussain, and A. Al-Durra, “Frequency regulation of hybrid shipboard microgrid system using butterfly optimization algorithm synthesis fractional-order controller,” International Journal of Numerical Modelling: Electronic Networks, Devices and Fields, vol. 36, no. 5. Wiley, August, 2022

[31] M. Dehghani, M. H. Khooban, T. Niknam, and S. M. R. Rafiei, “Time-Varying Sliding Mode Control Strategy for Multibus Low-Voltage Microgrids with Parallel Connected Renewable Power Sources in Islanding Mode,” Journal of Energy Engineering, vol. 142, no. 4. American Society of Civil Engineers (ASCE), Dec. 2016.

[32] S. Kayalvizhi and D. M. Vinod Kumar, “Load Frequency Control of an Isolated Micro Grid Using Fuzzy Adaptive Model Predictive Control,” IEEE Access, vol. 5. Institute of Electrical and Electronics Engineers (IEEE), pp. 16241–16251, 2017.

[33] M.-R. Chen, G.-Q. Zeng, Y.-X. Dai, K.-D. Lu, and D.-Q. Bi, “Fractional-Order Model Predictive Frequency Control of an Islanded Microgrid,” Energies, vol. 12, no. 1. MDPI AG, p. 84, Dec. 28, 2018.

[34] Yi Han, P. M. Young, A. Jain, and D. Zimmerle, “Robust Control for Microgrid Frequency Deviation Reduction with Attached Storage System,” IEEE Transactions on Smart Grid, vol. 6, no. 2. Institute of Electrical and Electronics Engineers (IEEE), pp. 557–565, Mar. 2015.

[35] R. K. Khadanga, A. Kumar, and S. Panda, “A modified Grey Wolf Optimization with Cuckoo Search Algorithm for load frequency controller design of hybrid power system,” Applied Soft Computing, vol. 124. Elsevier BV, p. 109011, July, 2022.

[36] B. Khokhar, S. Dahiya, and K. P. S. Parmar, “A Novel Hybrid Fuzzy PD-TID Controller for Load Frequency Control of a Standalone Microgrid,” Arabian Journal for Science and Engineering, vol. 46, no. 2. Springer Science and Business Media LLC, pp. 1053–1065, August. 28, 2020.

[37] A. Rai and D. K. Das, “The development of a fuzzy tilt integral derivative controller based on the sailfish optimizer to solve load frequency control in a microgrid, incorporating energy storage systems,” Journal of Energy Storage, vol. 48. Elsevier BV, p.103887, Apr. 2022.

[38] S. C. Sahoo, A. Kumar Barik, and D. C. Das, “Selfish-herd optimisation based frequency regulation in combined solar-thermal and biogas generator based hybrid microgrid,” 2020 International Conference on Contemporary Computing and Applications (IC3A) vol. 1. IEEE, pp. 330–335, February, 2020

[39] A. K. Barik and D. Chandra Das, “Optimal Load-frequency Regulation of BioRenewable Cogeneration based Interconnected Hybrid Microgrids with Demand Response Support,” 2018 15th IEEE India Council International Conference (INDICON). IEEE, Dec.2018.

[40] B. Khokhar, S. Dahiya, and K. P. Singh Parmar, “A Robust Cascade Controller for Load Frequency Control of a Standalone Microgrid Incorporating Electric Vehicles,” Electric Power Components and Systems, vol. 48, no. 6–7. Informa UK Limited, pp. 711–726, Apr. 20, 2020.

[41] S. A. M. Abdelwahab, W. S. E. Abdellatif, and A. M. Hamada, "Optimization of PID Controller for Hybrid Renewable Energy System Using Adaptive Sine Cosine Algorithm," International Journal of Renewable Energy Research (IJRER), vol. 10, no. 2, pp. 793-801, 2020. doi: 10.20508/ijrer. v10i2.10685.g7938.

[42] S. C. Sahoo, A. K. Barik, and D. C. Das, “A novel Green Leaf-hopper Flame optimization algorithm for competent frequency regulation in hybrid microgrids,” International Journal of Numerical Modelling: Electronic Networks, Devices and Fields, vol. 35, no. 3. Wiley, January, 2022.

[43] L. Wang, Q. Cao, Z. Zhang, S. Mirjalili, and W. Zhao, “Artificial rabbits optimization: A new bio-inspired meta-heuristic algorithm for solving engineering optimization problems,” Engineering Applications of Artificial Intelligence, vol. 114. Elsevier BV, p. 105082, Sep. 2022.

[44] A. K. Barik and D. C. Das, “Expeditious frequency control of solar photovoltaic/biogas/biodiesel generator based isolated renewable microgrid using grasshopper optimisation algorithm,” IET Renewable Power Generation, vol. 12, no. 14. Institution of Engineering and Technology (IET), pp. 1659–1667, Sep. 21, 2018.

[45] B. Yildirim, M. Gheisarnejad, and M. H. Khooban, “Delay-Dependent Stability Analysis of Modern Shipboard Microgrids,” IEEE Transactions on Circuits and Systems I: Regular Papers, vol. 68, no. 4. Institute of Electrical and Electronics Engineers (IEEE), pp. 1693–1705, Apr. 2021.

[46] S. A. M. Abdelwahab, W. S. E. Abdellatif, and A. M. Hamada, "Comparative Analysis of the Modified Perturb & Observe with Different MPPT Techniques for PV Grid Connected Systems," Int. J. Renew. Energy Res. (IJRER), vol. 10, no. 1, pp. 156-164, 2020.

[47] S. A. H. Naqvi, T. Taner, M. Ozkaymak, and H. M. Ali, “Hydrogen Production through Alkaline Electrolyzers: A Techno-Economic and Enviro-Economic Analysis,”

Chemical Engineering & Technology, vol. 46, no. 3. Wiley, pp. 474–481, October. 05, 2022.

[48] T. Taner, “Energy and exergy analyze of PEM fuel cell: A case study of modeling and simulations,” Energy, vol. 143. Elsevier BV, pp. 284–294, January. 2018.

[49] T. Taner, “The novel and innovative design with using H2 fuel of PEM fuel cell: Efficiency of thermodynamic analyze,” Fuel, vol. 302. Elsevier BV, p. 121109, October. 2021.

[50] I. Ngamroo, “Application of electrolyzer to alleviate power fluctuation in a standalone microgrid based on an optimal fuzzy PID control,” International Journal of Electrical Power & Energy Systems, vol. 43, no. 1. Elsevier BV, pp. 969–976, Dec. 2012.

[51] M. Regad, M. Helaimi, R. Taleb, A. M. Othman, and H. A. Gabbar, "Frequency Control in Microgrid Power System with Renewable Power Generation Using PID Controller Based on Particle Swarm Optimization," in Proceedings of the International Conference on Renewable Energy Research and Applications (ICRERA), 2020, pp. 3–13

[52] Y. Liu et al., “A Novel Adaptive Model Predictive Control for Proton Exchange Membrane Fuel Cell in DC Microgrids,” IEEE Transactions on Smart Grid, vol. 13, no. 3. Institute of Electrical and Electronics Engineers (IEEE), pp. 1801–1812, May 2022.

[53] T. Taner, S. A. H. Naqvi, and M. Ozkaymak, “Techno-economic Analysis of a More Efficient Hydrogen Generation System Prototype: A Case Study of PEM Electrolyzer with Cr-C Coated SS304 Bipolar Plates,” Fuel Cells, vol. 19, no. 1. Wiley, pp. 19–26, January, 2019.

[54] V. L. Sanches, M. R. da C. M. Aguiar, M. A. V. de Freitas, and E. B. A. V. Pacheco, “Management of cruise ship-generated solid waste: A review,” Marine Pollution Bulletin, vol. 151. Elsevier BV, p. 110785, February 2020.

[55] F. F. Angkasa, R. Zafar, and I.-Y. Chung, “Optimal Power Generation and Voltage Scheduling in Shipboard Power Systems Considering Load Characteristics-Based Operating Reserve Management,” Journal of Electrical Engineering & Technology, vol. 18, no. 4. Springer Science and Business Media LLC, pp. 2505–2515, June, 2023.

[56] O. A. Ahmed and J. A. M. Bleijs, “Power flow control Methods for an ultracapacitor bidirectional converter in DC microgrids—A comparative study,” Renewable and Sustainable Energy Reviews, vol. 26. Elsevier BV, pp. 727–738, October, 2013.

[57] D. Rekioua, K. Kakouche, A. Babqi, Z. Mokrani, A. Oubelaid, T. Rekioua, and S. A. M. Abdelwahab, “Optimized Power Management Approach for Photovoltaic Systems with Hybrid Battery-Supercapacitor Storage,” Sustainability, vol. 15, no. 19, pp. 14066, 2023. doi: 10.3390/su151914066.

[58] B. Khokhar, S. Dahiya, and K. P. S. Parmar, “A novel hybrid fuzzy PD-TID controller for load frequency control of a standalone microgrid,” in Proc. Int. Conf. Smart Grid (icSmartGrid), 2021, pp. 56–62.

[59] D. K. I. Alham, “Enhancing the conventional controllers for load frequency control of isolated microgrids using artificial rabbits optimization algorithm,” Int. J. Smart Grid, vol. 7, no. 3, pp. 112–120, 2023.

[60] M. Gheisarnejad and M. H. Khooban, “Secondary load frequency control for multi-microgrids: HiL real-time simulation,” in Proc. Int. Conf. Renew. Energy Res. Appl. (ICRERA), 2019, pp. 1–6.